Available online at www.sciencedirect.com
SCIENCE DIRECT®
Journal of Solid State Chemistry 177 (2004) 701–708
JOURNAL OF SOLID STATE CHEMISTRY
http://elsevier.com/locate/jssc

A low-temperature electron diffraction study of structural disorder and its relationship to the Kondo effect in ThAsSe

R.L. Withers,[a,*] R. Vincent,[b] and J. Schoenes[c]

[a] *Research School of Chemistry, Australian National University, Canberra ACT 0200, Australia*
[b] *H.H. Wills Physics Laboratory, University of Bristol, Bristol BS8 1TL, UK*
[c] *Institute for Semiconductor Physics and Optics, Technical University Braunschweig, D-38106 Braunschweig, Germany*

Received 15 May 2003; received in revised form 10 August 2003; accepted 20 August 2003

Abstract

A low-temperature electron diffraction study has been carried out on ThAsSe to search for evidence of structural disorder associated with the low-temperature non-magnetic Kondo effect. A highly structured and extremely complex characteristic diffuse intensity distribution has been observed at low temperature and interpreted in terms of a gradual charge density wave type phase transition upon lowering of temperature involving disordered As–As dimerization within (001) planes. Plausible models of the proposed As–As dimerization have been obtained using a group theoretical approach.

Keywords: Kondo effect; As dimerization; Charge density wave; Transmission electron microscopy; Incommensurately modulated

1. Introduction

The specific electrical resistivity of UAsSe displays negative $d\rho/dT$ temperature coefficients of resistivity between 2 and 50 K and again above 109 K over a range of several hundred degrees Kelvin [1]. Ever since the initial discovery of these unusual low-temperature transport properties in UAsSe, there has been much interest in the Kondo scattering mechanism/s responsible [1–10]. The fact that UAsSe becomes ferromagnetic below $T_c \sim 110$ K [2] initially suggested a scattering mechanism of magnetic origin related to the original Kondo effect [11]. Early investigations thus concentrated on the determination of the low-temperature magnetic structure and its relation to the electronic structure [2–6].

The subsequent discovery that diamagnetic ThAsSe (of the same ZrSiS average structure type as UAsSe—see Fig. 1) displayed qualitatively very similar behavior to UAsSe (above 109 K) with negative $d\rho/dT$ from about 70 up to about 500 K [1], however, ruled out a scattering mechanism of magnetic origin. More recent examination of the magnetoresistivity of UAsSe at liquid He temperature [8–10] likewise suggests that the dominant scattering mechanism in both materials is of a structural rather than magnetic origin.

Several types of non-magnetic Kondo scattering mechanisms have been proposed for these materials including the condensation of a charge density wave (CDW) [1,12], a quadrupolar Kondo model for the U^{4+} ion in cubic symmetry [10,13] and a positionally disordered two-level system (TLS) Kondo model [10,14]. The precise structural origin of the assumed two-state local positional disorder of the latter TLS model [14] is nowhere spelt out although the anomalously large anisotropic displacement parameters of all constituent atoms is certainly consistent with positional disorder of some sort [10]. Some authors have linked it to the recently discovered partial As/Se anion disorder in UAsSe [8] despite the fact that no such equivalent As/Se disorder has been reported for ThAsSe.

Hall-effect measurements show that the low-temperature increase in basal plane resistivity of ThAsSe is due to a reduction of the carrier concentration by roughly one order of magnitude from $\sim 0.6\,e^-$ per formula unit (f.u.) at room temperature to $0.08\,e^-$/f.u. at and below 100 K [1]. Given that basal plane conductivity is primarily due to hole delocalization within the (001) planes of As ions, the most likely candidate responsible

*Corresponding author. Fax: +612-612-50750.
E-mail address: withers@rsc.anu.edu.au (R.L. Withers).

0022-4596/$ - see front matter © 2003 Elsevier Inc. All rights reserved.
doi:10.1016/j.jssc.2003.08.032

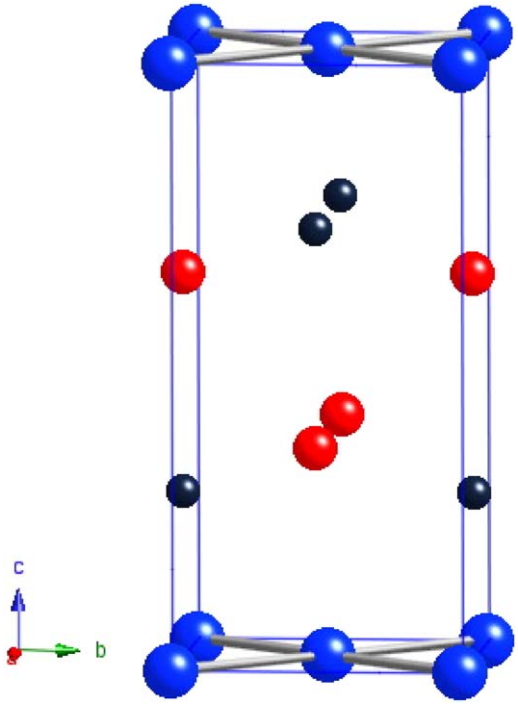

Fig. 1. Shows the $P4/nmm$ (Origin Choice 2), ZrSiS-type average structure of ThAsSe projected close to [100]. The As atoms are represented by the large blue balls, the Th ions by the small black balls and the Se ions by the medium-sized red balls. The covalent bonding between the As atoms is represented by the gray rods.

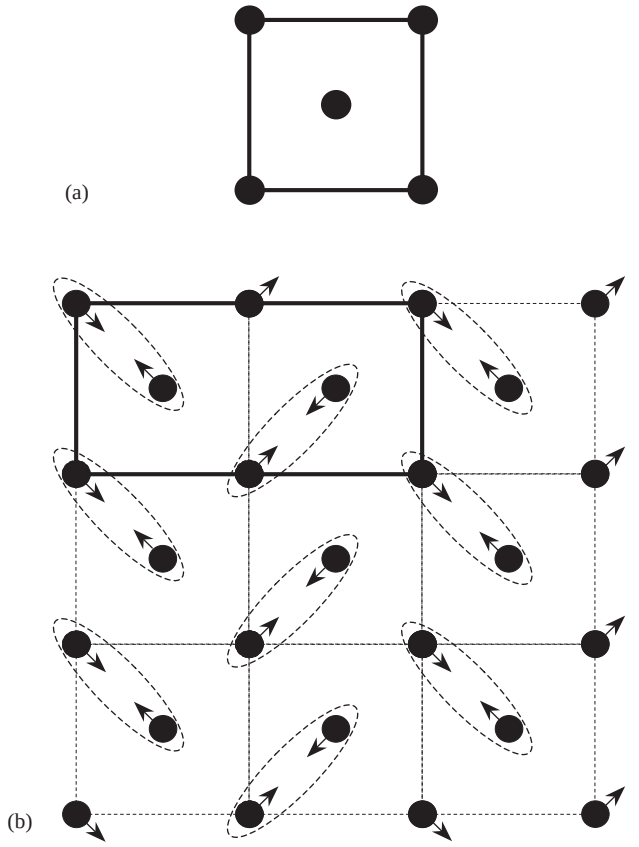

Fig. 2. (a) The (001) plane of As ions in ThAsSe. This also represents the (001) plane of Se ions in the underlying average structure of $LaSe_2$ [25]. The underlying tetragonal parent unit cell in each case is represented by the solid lines. (b) The characteristic herring-bone pattern of $(Se_2)^{2-}$ dimerization within the parent (001) planes of $LaSe_2$ (adapted from Fig. 2 of [25]).

would appear to be the gradual formation of a CDW involving As–As dimerization as temperature is lowered. Dimerization of the anions in the As position is a common feature of compounds crystallizing in the family of ZrSiS-related structures [15] (see e.g., Fig. 2). Local As–As dimerization of this sort would clearly reduce the hole carrier concentration and hence the overall conductivity. Schoenes et al. [1] thus originally proposed a gradual phase transition from an essentially metallic ThAsSe (of ZrSiS structure type) without any As–As bonding at high temperature to a tending towards insulating (the basal plane resistivity of ThAsSe reaches values as high as $450\,\mu\Omega\,cm$ [1] at low temperature) $Th_2^{4+}(As_2)^{4-}Se_2^{2-}$ with $(As–As)^{4-}$ covalently bonded dimers (the covalent As–As single bond diameter is ~ 2.44 Å) at low temperature.

The characteristic signature of a condensed CDW is normally thought to be the existence of additional satellite reflections below some usually well-defined phase transition temperature [12,16]. In the case of UAsSe and ThAsSe, however, the absence of any sharp resistivity anomaly as a function of temperature suggests that no such well-defined CDW phase transition exists [1]. Broad resistivity anomalies of the type observed are thought to be more typical of order–disorder phase transitions. Nevertheless, both the CDW mechanism and the TLS model imply the existence of positional disorder which should give rise to weak additional scattering in addition to the strong Bragg reflections of the underlying ZrSiS average structure type.

Given the well-known sensitivity of electron diffraction to weak features of reciprocal space [17] (and despite the failure of previous primarily HREM investigations to detect anything out of the ordinary [8,10]), a low-temperature transmission electron microscope (TEM) investigation of ThAsSe was therefore carried out to search for some evidence of structural distortion, associated either with a CDW or with anion disorder. The purpose of the current paper is to present the results of this low-temperature electron diffraction investigation of ThAsSe.

2. Experimental

2.1. Synthesis

The as-grown single-crystal specimens of ThAsSe investigated in this study ($a = 4.081(3)$, $c = 8.562(5)$ Å) were grown by Dr. F. Hulliger at ETH, Zürich. The

synthesis procedure is described in Ref. [18]. The crystals took the form of thin plates perpendicular to the **c**-axis of the ZrSiS average structure type. Specimens suitable for observation in the TEM were obtained by cleavage. The resultant specimens took the form of thin plates perpendicular to **c** which severely limited the accessible range of available zone axis orientations. The specimens were examined in a Philips EM430 TEM operating at 200 kV. A liquid He cold stage was used for the low-temperature work.

2.2. TEM

Fig. 3a shows a typical [001] zone axis electron diffraction pattern (EDP) of ThAsSe taken at 100 K. A virtually identical pattern was also obtained at 30 K. The strong, sharp Bragg reflections of the underlying, nominally $P4/nmm$ average structure (see Fig. 1) are clearly present although there is some evidence for very weak symmetry breaking in the extremely weak presence (close in to the centre of Fig. 3a) of n glide forbidden $hk0$, $h+k$ odd reflections such as $[100]^*$ and $[010]^*$. In addition to these strong parent Bragg reflections, note the presence of a spectacular and highly structured characteristic diffuse intensity distribution in the form of two orthogonal $\mathbf{G}\pm\sim 0.14\langle 1\bar{1}0\rangle^*\pm\varepsilon\langle 110\rangle^*$ (ε continuous) 'lines' of diffuse streaking running along the $\langle 110\rangle^*$ directions of reciprocal space around the nominally n glide forbidden $hk0$, $h+k$ odd reflections. (In what follows, we label as **G** the family of Bravais lattice allowed Bragg reflections of the parent structure, including the nominally n glide forbidden $hk0$, $h+k$ odd reflections.) The fact that the $\mathbf{G}\pm\sim 0.14\langle 1\bar{1}0\rangle^*\pm\varepsilon\langle 110\rangle^*$ diffuse streaking in Fig. 3a occurs only around the $\mathbf{G}=[hk0]^*$, $h+k$ odd, but not even, reflections is an 'extinction condition' characteristic of the disordered phase and places constraints on the possible displacive shifts responsible (see, for example, Ref. [19] and below).

At the intersection points of these orthogonal diffuse lines apparent incommensurate satellite reflections characterized by the primary modulation wave vectors $\mathbf{q}_1\sim 0.28\mathbf{a}^*$ and $\mathbf{q}_2\sim 0.28\mathbf{b}^*$, respectively, occur. (A two–dimensional (2-D) 'long-range ordered' superstructure appears to be attempting to condense out. The phenomenon of satellite reflections condensing out onto and/or coexisting with extended continuous diffuse distributions while unusual is by no means unknown as, for example, in the cases of the $1T_1$ polymorph of TaS_2 (see, for example, Fig. 9 of Ref. [16]) or the ceramic mullite [20]. In the case of TaS_2, the condensation process is completed as temperature is lowered, i.e., the diffuse distribution disappears altogether on cooling sufficiently leaving only sharp satellite reflections [21]. In the current case, however, the incommensurate 'satellite reflections' and the continuous diffuse lines continue to coexist right down to the lowest temperature obtainable, 30 K). There is once more an 'extinction condition' in the sense that the $\mathbf{G}\pm\mathbf{q}_1$ and $\mathbf{G}\pm\mathbf{q}_2$ satellite reflections again occur around the $\mathbf{G}=[hk0]^*$, $h+k$ odd, but not even, reflections. Note also the remarkable shape (somewhat like a small amplitude 'vibrating skipping rope') of the diffuse 'lines' in the larger regions between

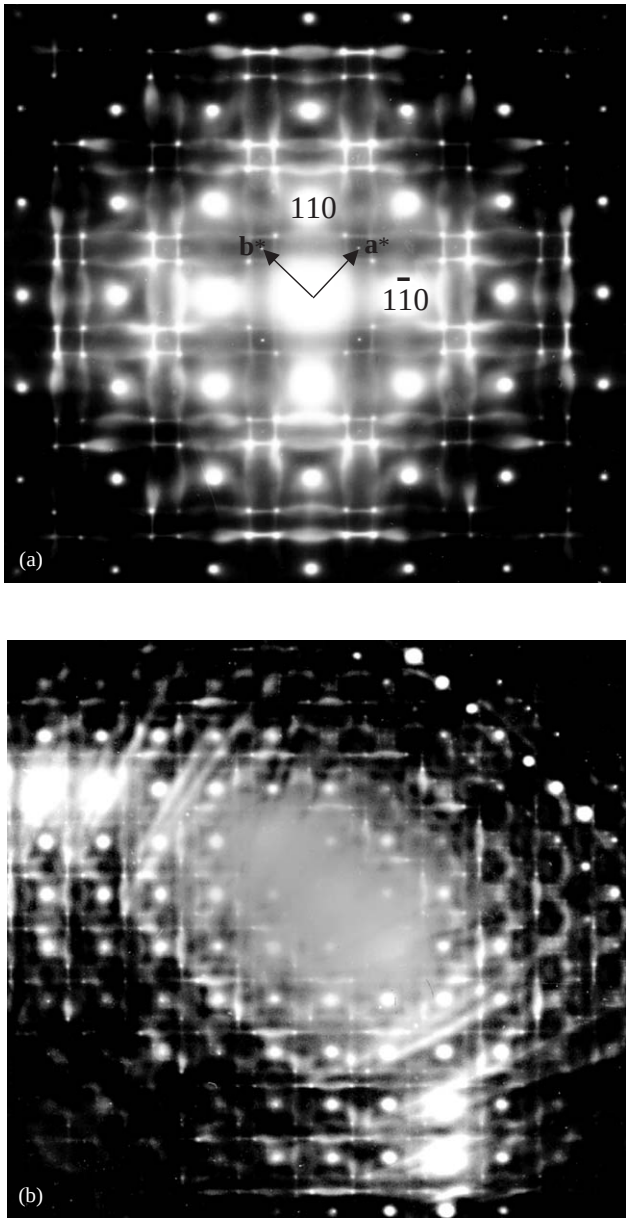

Fig. 3. (a) A typical [001] zone axis EDP of ThAsSe taken at 100 K. In addition to the strong Bragg reflections of the underlying $P4/nmm$ average structure, note the presence of a spectacular and highly structured characteristic diffuse intensity distribution in the form of two orthogonal 'lines' of diffuse streaking running along the $\mathbf{G}\pm\sim 0.14\langle 1\bar{1}0\rangle^*\pm\varepsilon\langle 110\rangle^*$ positions of reciprocal space around the nominally n glide forbidden $hk0$, $h+k$ odd reflections. (b) A close to [001] zone axis EDP of ThAsSe again taken at 100 K obtained by tilting a few degrees away from the exact [001] zone axis orientation to reduce double diffraction effects apparent in (a).

the 'satellite reflections' as well as the enhanced intensity of the diffuse scattering inside the {400} Kikuchi bands.

The transverse polarized nature (see e.g., Ref. [22]) of the intensity distribution associated with both the diffuse 'lines' as well as the 'satellite reflections', e.g., the $\mathbf{G}\pm\sim 0.14\langle 1\bar{1}0\rangle^*\pm\varepsilon\langle 110\rangle^*$ diffuse 'lines' are most intense when looking out along the $\langle 1\bar{1}0\rangle^*$ direction of reciprocal space and weakest along the orthogonal $\langle 110\rangle^*$ direction (particularly towards the edge of Fig. 2a) whilst the $\mathbf{G}\pm\sim 0.28\langle 100\rangle^*$ satellite reflections are most intense for $\mathbf{G}$ running along $\langle 010\rangle^*$ and have zero intensity for $\mathbf{G}$ running along $\langle 100\rangle^*$ is also apparent.

The polarization effect associated with the diffuse 'lines' is somewhat blurred in Fig. 2a as a result of double diffraction particularly close in to the center of the pattern. It is easier to recognize upon tilting a few degrees away from the exact [001] zone axis orientation (to reduce multiple scattering effects) as shown in Fig. 2b. (Such a strong polarization effect requires that the dominant contribution to the observed scattering arises from atom displacements away from the underlying average structure positions of Fig. 1). Also most apparent in Fig. 3b is the presence of a strongish 'size effect' [23] in the asymmetric intensity distribution of the $\mathbf{G}\pm\sim 0.14\langle 1\bar{1}0\rangle^*\pm\varepsilon\langle 110\rangle^*$ lines with the lines on the high angle side of the particular Bragg reflection $\mathbf{G}$ always being stronger in intensity than the parallel lines on the low angle side. Such an 'atomic size effect' is a characteristic of systems displaying relatively large displacive relaxations [19,23]. A further weaker type of curved diffuse distribution is also apparent in Fig. 3b in the region between the zero-order Laue zone (ZOLZ) and the first OLZ of reflections.

The fact that the $\mathbf{G}\pm\sim 0.14\langle 1\bar{1}0\rangle^*\pm\varepsilon\langle 110\rangle^*$ 'lines' of diffuse intensity in Fig. 3a extend so far in Fig. 3b suggests that they may in fact not be lines but rather part of an essentially continuous plane of diffuse intensity perpendicular to each of the two $\langle 110\rangle$ real space directions. This is confirmed by the [101] zone axis EDP shown in Fig. 4. This EDP was obtained by tilting $\sim 25^\circ$ away from the [001] zone axis orientation of Fig. 3a around the $[020]^*$ systematic row. Note that the strong transverse polarized diffuse streaking apparent in Fig. 3 (even down to the 'vibrating string' shape) is still present but this time runs along the $[\bar{1}11]^*$ (perpendicular to the [110] real space direction) and $[11\bar{1}]^*$ (perpendicular to $[1\bar{1}0]$) reciprocal space directions and remains present no far how we tilt around the $[020]^*$ systematic row. Clearly, the diffuse takes the form of continuous sheets of diffuse intensity perpendicular to the [110] and $[1\bar{1}0]$ directions, respectively.

The polarized nature of the diffuse streaking apparent in Figs. 3 and 4 requires that the dominant contribution to the diffuse sheet perpendicular to [110] arises from atomic displacements along [110] in real space while the dominant contribution to the diffuse sheet perpendicular to $[1\bar{1}0]$ arises from atomic displacements along $[1\bar{1}0]$. Note again the presence of apparent 'satellite reflections' where the diffuse streaks intersect in Fig. 4 giving rise this time to $\mathbf{G}\pm\mathbf{q}'_1(\mathbf{q}'_1\sim 0.28[\bar{1}01]^*)$ (one such 'reflection' is arrowed in the bottom right-hand corner of Fig. 4) and $\mathbf{G}\pm\mathbf{q}_2(\mathbf{q}_2\sim 0.28b^*)$ satellite reflections. Clearly, the 'satellite reflections' of Fig. 3a are in fact part of a continuous rod of diffuse intensity running along the $\mathbf{c}^*$ direction of reciprocal space. Finally, note once more the transverse polarized nature of the intensity distribution associated with these 'satellite reflections', e.g., the $\mathbf{G}\pm\sim 0.28[\bar{1}01]^*$ satellite reflections are most intense for $\mathbf{G}$ running along $[020]^*$ and have zero intensity for $\mathbf{G}$ running perpendicular to $[020]^*$ whilst the $\mathbf{G}\pm\sim 0.28[010]^*$ satellite reflections are most intense for $\mathbf{G}$ running along $[\bar{1}01]^*$ and have zero intensity for $\mathbf{G}$ running along $[020]^*$ in Fig. 4.

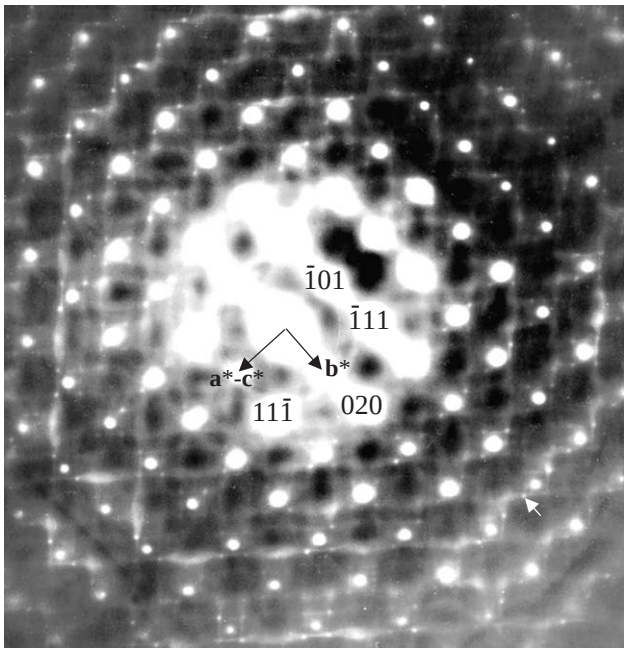

Fig. 4. A [101] zone axis EDP of ThAsSe again taken at 100 K and obtained by tilting $\sim 25^\circ$ away from the [001] zone axis orientation of Fig. 2a around the $[020]^*$ systematic row. A $\mathbf{G}\pm\mathbf{q}'_1(\mathbf{q}'_1\sim 0.28[\bar{1}01]^*)$ 'reflection' is arrowed in the bottom right-hand corner.

3. Interpretation

$\{110\}^*$ sheets of diffuse intensity in reciprocal space imply the existence of $\langle 110\rangle$ rods of atoms in real space exhibiting displacements correlated along $\langle 110\rangle$ but with essentially no correlation from one such rod to the next in the plane perpendicular to the rod direction (see e.g., Ref. [22]). The observed polarization behavior of the diffuse sheets (see Figs. 3 and 4) requires that the displacement direction of the atoms within these $\langle 110\rangle$

correlated rods must also be along $\langle 110 \rangle$. Likewise the closely related $[0.28, 0, l]^*$ and $[0, 0.28, l]^*$ rods of diffuse intensity in reciprocal space [24] imply the existence of two-dimensionally ordered or correlated (001) planes of atoms in real space exhibiting correlated atomic displacements (along [010] and [100], respectively) within the plane but with no correlation from one such (001) plane to the next.

Given the Hall-effect evidence discussed earlier, the most likely candidate responsible for the observed diffuse scattering would appear to be the dimerization (or covalent bonding) of As–As nearest neighbors along local $\langle 110 \rangle$ directions within (001) planes (see e.g., Fig. 2). The already quite short average As–As nearest neighbor separation distance (of $\frac{1}{2}\langle 110 \rangle \sim 2.888$ Å) within the (001) planes of the underlying ZrSiS-type average structure (see Fig. 1) is compatible with such a proposal as is the experimentally observed $\langle 110 \rangle$ direction of the displacement eigenvectors associated with the $\{110\}^*$ sheets of diffuse intensity and the extinction condition represented by the fact that both the 'satellite reflections' and the diffuse streaking in Fig. 3a only occur around the n glide forbidden $h\,k\,0$, $h + k$ odd parent reflections (see below for more detail).

The continuous nature along $\mathbf{c}^*$ of the diffuse streaking and 'satellite reflections' of Fig. 3a requires that there be no correlation from one (001) As plane to the next along the $\mathbf{c}$ direction of either the one-dimensional (1-d) $\langle 110 \rangle$ As–As dimerization strings implied by the $\{110\}^*$ diffuse sheets or the 2-d (001) As–As dimerization patterns implied by the rods of diffuse intensity. This is not unreasonable given the relatively large $\mathbf{c}$-axis dimension of ~ 8.6 Å. Despite this inherent disorder, a progressive increase in the extent of As–As dimerization within each of the individual (001) As planes upon lowering of temperature would explain the Hall-effect evidence for a reduction by almost an order of magnitude in carrier concentration on lowering of temperature to 100 K. A model along these lines was proposed by Schoenes et al. [1] many years ago on purely crystal chemical grounds but without any direct diffraction evidence. The gradual diminution of the diffuse intensity upon increasing temperature is compatible with such a proposal.

Such covalently bonded chalcogenide–chalcogenide dimerization is a common feature of the crystal chemistry of chalcogenides (see e.g., [25,26]). It usually, however, leads to a long-range ordered superstructure phase as, for example, in the closely related case of $LaSe_2$ [25] (see, for example, Fig. 2b) where $(Se_2)^{2-}$ dimers are packed in a characteristic herring-bone pattern within (001) planes (thereby doubling one or other of the originally tetragonal basal plane axes) which are also ordered from one such [001] plane to the next. In the present case, however, there is no evidence for a three-dimensionally long-range ordered superstructure phase even at the lowest possible temperatures. There is, however, evidence for a 2-d superstructure phase attempting to condense out, albeit incompletely (see Fig. 3a).

4. Patterns of As–As dimerization

Given the extent and complexity of the observed disorder (see Figs. 3 and 4), it is not possible to 'solve' for the low-temperature structure. It is, however, possible to generate plausible models for the As–As patterns of dimerization that we believe are primarily responsible for both the diffuse sheets and the diffuse rods using a (flexible) group theoretical or superspace approach (see, for example, Refs. [27–31] and Figs. 5 and 6) as follows.

4.1. The 1-d $\langle 110 \rangle$ As–As dimerization pattern

Consider firstly the 1-d (in real space) $\langle 110 \rangle$ As–As dimerization pattern associated with the observed $\mathbf{G} \pm \sim 0.14\langle 110 \rangle^* \pm \varepsilon\langle 1\bar{1}0 \rangle^* \pm \eta[001]^*$ (ε and η essentially continuous) sheets of diffuse intensity. $\{110\}^*$ sheets of diffuse intensity in reciprocal space imply the existence of $\langle 110 \rangle$ rods of atoms in real space exhibiting displacements correlated along $\langle 110 \rangle$ but with essentially no correlation from one such rod to the next in the plane perpendicular to the rod direction. Given the observed polarization behavior of these diffuse sheets, they arise from longitudinal $\langle 110 \rangle$ shifts of As ions along the $\langle 110 \rangle$ correlation direction associated with the 'primary modulation wave vector' $\mathbf{q} \sim 0.14\langle 110 \rangle^*$ [28,30].

Formally, there exist two distinct As sites per parent $P4/nmm$ unit cell: As1 at 000 and As2 at $\frac{1}{2}, \frac{1}{2}, 0$ (see Fig. 1). The fact that the $\mathbf{G} \pm \mathbf{q} \pm \varepsilon\langle 1\bar{1}0 \rangle^*$ diffuse streaking in Fig. 3a occurs only around the $\mathbf{G} = [hk0]^*$, $h + k$ odd, but not even, reflections is formally equivalent to the condition $F(h\,k\,0\,m \equiv h\mathbf{a}^* + k\mathbf{b}^* + l\mathbf{c}^* + m\mathbf{q}) = 0$ unless m is even. In superspace terms, it implies the existence of the superspace symmetry operation $\{x_1 + \frac{1}{2}, x_2 + \frac{1}{2}, -x_3, x_4 + \frac{1}{2}\}$ and requires the As1 and As2 shifts along $\langle 110 \rangle$ to be out of phase. The most general possible displacive atomic modulation functions (AMFs; [28, 30]) for these As ions compatible with the experimental observations is then given by:

$$\mathbf{U}_{\mathrm{As1,2}}(\bar{x}_4 = \mathbf{q} \cdot [\mathbf{r}_{\mathrm{As1,2}} + \mathbf{t}]) = \pm\varepsilon_{\mathrm{As}}(\mathbf{a} + \mathbf{b})\cos 2\pi(\bar{x}_4 - \phi) + \cdots \text{ higher order harmonic terms}\ldots, \quad (1)$$

where the '+' sign refers to the As1 atoms, the '−' sign to the As2 atoms, $\mathbf{q} \sim 0.14\langle 110 \rangle^*$ and ϕ represents the so-called global phase [28,31].

Experimentally, only the first-order $\mathbf{G} \pm \mathbf{q}$ diffuse sheets are observed (see Fig. 3a). This could be interpreted as implying either a sinusoidal AMF or,

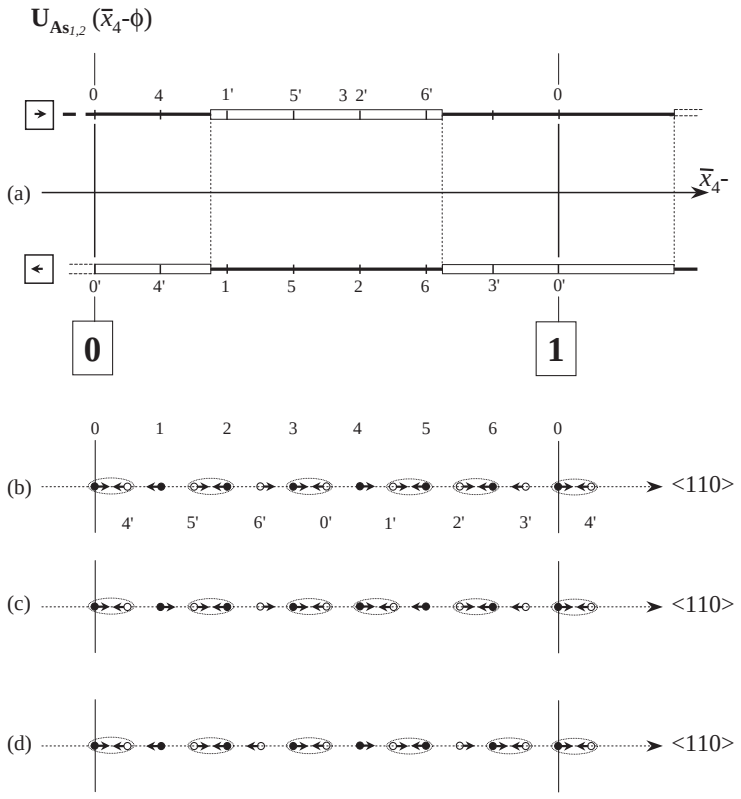

Fig. 5. (a) Shows the square wave As1,2 displacive AMFs along the $(\bar{x}_4 - \phi)$ direction of superspace (the solid line represents the assumed displacive AMF of As1 while the 180° out of phase displacive AMF of As2 is represented by the open bar square wave). Note that $\bar{x}_4 = \mathbf{q}\cdot[\mathbf{r}_{As1,2} + \mathbf{t}]$, where $\mathbf{q} \sim 0.14\langle 110\rangle^*$, $\mathbf{r}_{As1} = \mathbf{0}$, $\mathbf{r}_{As2} = \frac{1}{2}\langle 110\rangle$, $\mathbf{t} = m\langle 110\rangle$, m an integer and ϕ is the global phase. The resultant predicted 1-d As–As dimerization pattern assuming $\phi = 0$ and $\mathbf{q} = \frac{1}{7}\langle 110\rangle^*$ exactly is shown in (b). The equivalent, phason shifted $\langle 110\rangle$ As–As dimerization patterns assuming $\phi = +\frac{1}{14}$ and $-\frac{1}{14}$, respectively, are shown in Figs. 5c and d. As–As dimers are circled in (b)–(d).

alternatively, a more square-wave-like AMF but with some considerable degree of phason (global phase) wobble. For the purposes of deriving a plausible As–As dimerization pattern, we have made the latter assumption and assumed an inherently square-wave shape for the above displacive AMF (see Fig. 5a), i.e., for $-\frac{1}{4} < (\bar{x}_4 - \phi) < \frac{1}{4}$ along the $(\bar{x}_4 - \phi)$ direction of hyperspace we ascribe a value of $+1$ to $\cos 2\pi(\bar{x}_4 - \phi)$ in Eq. (1) above and for $+\frac{1}{4} < (\bar{x}_4 - \phi) < \frac{3}{4}$ we ascribe a value of -1.

The resultant predicted As–As dimerization pattern assuming $\phi = 0$ and $\mathbf{q} = \frac{1}{7}\langle 110\rangle^*$ exactly is shown in Fig. 5b. The equivalent, phason shifted $\langle 110\rangle$ As–As dimerization patterns assuming $\phi = +\frac{1}{14}$ and $-\frac{1}{14}$, respectively, are shown in Figs. 5c and d. Note that the sign of the shifts of only two out of the 14 As ions in the resultant seven times supercell, i.e., As1 and 1′, have flipped in going from Figs. 5b to c while the signs of As6 and 6′ have flipped in going from Figs. 5b to d. It is not difficult to imagine such sort of flipping going on along any particular $\langle 110\rangle$ chain and thus smearing the observed AMF shape from square wave like to more sinusoidal. We thus believe that Fig. 5b (or c or d) give entirely plausible 1-d As–As patterns of dimerization primarily responsible for the existence of the observed sheets of diffuse intensity.

The next question is what sort of As–As dimerization pattern could be responsible for the observed diffuse rods at the intersection of the orthogonal diffuse sheets?

4.2. 2-d (001) As–As dimerization patterns

If we ignore the existence of the diffuse sheets and concentrate instead purely on the $\mathbf{q}_1'' = 0.28\mathbf{a}^* + l\mathbf{c}^*$ and $\mathbf{q}_2'' = 0.28\mathbf{b}^* + l\mathbf{c}^*$ diffuse rods it is again possible to generate a picture of the sort of As–As pattern of dimerizations responsible using a group-theoretical or superspace-type approach [27] (see Fig. 6b). In order to generate such a distribution, however, it is again first necessary to use group theoretical considerations to appropriately constrain the possible As–As dimerization patterns as follows.

A general condensed phonon mode with modulation wave vector $\mathbf{q}_1'' \sim 0.28\mathbf{a}^* + l\mathbf{c}^*$ has a little co-group [29] consisting of only two elements, the identity E and the mirror perpendicular to $\mathbf{b}$, m_y. Under the parent symmetry operations $\{m_x|\mathbf{0}\}$ or $\{m_y|\mathbf{0}\}$, the two independent As ions per parent unit cell, As1 and As2,

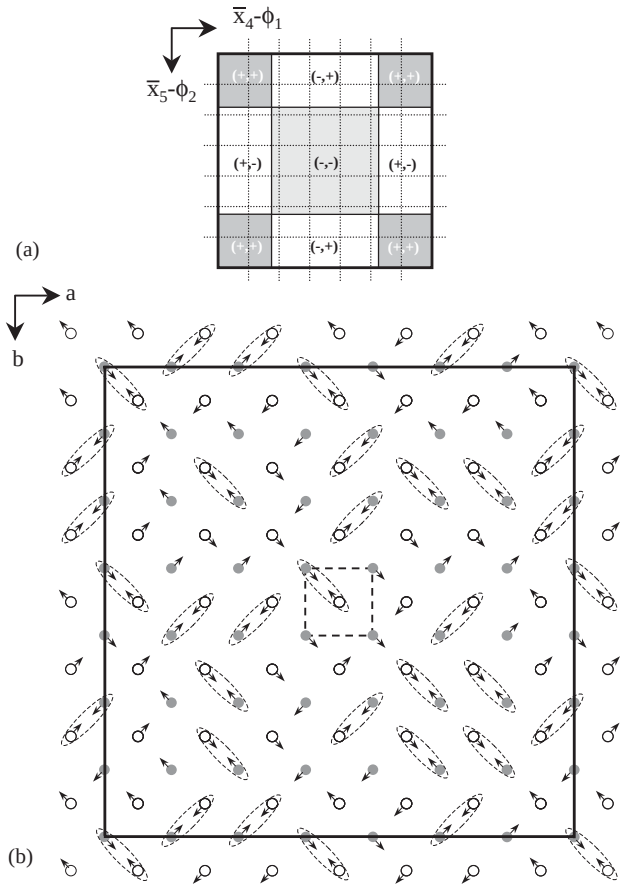

Fig. 6. (a) Shows the assumed 2-d square wave As1,2 displacive AMFs as functions of $(\bar{x}_4-\phi_1)$ and $(\bar{x}_5-\phi_2)$ (see Eq. (2) in the text). The local + or − values of the square wave variables in (a) are represented by the pair of + and − values in the different regions of superspace. Note that $\bar{x}_4=\mathbf{q}_1\cdot[\mathbf{r}_{As1,2}+\mathbf{t}]$ and $\bar{x}_5=\mathbf{q}_2\cdot[\mathbf{r}_{As1,2}+\mathbf{t}]$, where $\mathbf{q}_1\sim0.28\mathbf{a}^*$ and $\mathbf{q}_2\sim0.28\mathbf{b}^*$, $\mathbf{r}_{As1}=\mathbf{0}$, $\mathbf{r}_{As2}=\frac{1}{2}(\mathbf{a}+\mathbf{b})$, $\mathbf{t}=m\mathbf{a}+n\mathbf{b}$, m, n integers and ϕ_1 and ϕ_2 are global phases. The resultant predicted $7\mathbf{a}\times7\mathbf{b}$ As–As dimerization pattern assuming ϕ_1 and ϕ_2 are both = 0, $\mathbf{q}_1=\frac{2}{7}\mathbf{a}^*$ and $\mathbf{q}_2=\frac{2}{7}\mathbf{b}^*$ exactly is shown in (b). The As1 ions are represented by the filled circles and the As2 ions by the open circles.

each map into themselves modulo a Bravais lattice vector. A character of −1 under $\{m_y|\mathbf{0}\}$ for such a condensed phonon mode thus implies that As1 and As2 can each only move in the **b** direction, i.e., $\mathbf{e}_{As1,2}(\mathbf{q}_1'')$ must be along **b**. The very clear transverse polarized nature of the observed intensity distribution of the 'satellite reflections' in Fig. 3a (as well as Fig. 4) is entirely consistent with such a transverse polarized displacement eigenvector regardless of the value of l.

The atomic displacements responsible (assumed from here on in to be primarily As displacements $\mathbf{e}_{As1,2}(\mathbf{q}_{1,2}''))$ associated with the modulation wave vectors $\mathbf{q}_1''\sim0.28\mathbf{a}^*+l\mathbf{c}^*$ and $\mathbf{q}_2''\sim0.28\mathbf{b}^*+l\mathbf{c}^*$ must then run along **b** and **a**, respectively, i.e., $\mathbf{e}_{As1,2}(\mathbf{q}_1)$ must be parallel to **b** and $\mathbf{e}_{As1,2}(\mathbf{q}_1)$ must be parallel to **a**. The equivalent statement in the language of superspace is to say that there exist superspace symmetry operations $\{-x_1,+x_2,x_3,-x_4+2\phi_1,+x_5+\frac{1}{2}\}$ and $\{+x_1,-x_2,x_3,+x_4+\frac{1}{2},-x_5+2\phi_2\}$, respectively. Such superspace symmetry operations imply characteristic extinction conditions given by $F(0kl0n)=0$ unless $n=2J$ and $F(h0lm0)=0$ unless $m=2J$ (m, n, J all integers). Unfortunately, because of the layered nature of the cleaved material investigated, we were not able to obtain [100] or [010] zone axis EDPs to confirm these predicted extinction conditions. The absence of $\mathbf{G}\pm0.28\mathbf{a}^*+l\mathbf{c}^*$ diffuse streaking in previously published [010]-type EDPs of crushed samples of ThAsSe [10] is however consistent with such a superspace symmetry operation.

If we ignore the $\mathbf{c}^*$ components of the above primary modulation wave vectors and focus on the $\mathbf{q}_1\sim0.28\mathbf{a}^*$ and $\mathbf{q}_2\sim0.28\mathbf{b}^*$ modulation waves alone, i.e., we index Fig. 3a using the five basis vectors $M^*=\{\mathbf{a}^*,\mathbf{b}^*,\mathbf{c}^*,\mathbf{q}_1=\varepsilon\mathbf{a}^*,\mathbf{q}_2=\varepsilon\mathbf{b}^*$ with $\varepsilon=0.28\sim\frac{2}{7}\}$, then the only observed characteristic extinction condition is given by $F(h\,k\,0\,m\,n)=0$ unless $h+k+m+n=2J$, h,k,m,n,J all integers (see Fig. 3a) corresponding to the superspace glide operation $\{x_1+\frac{1}{2},x_2+\frac{1}{2},-x_3,x_4+\frac{1}{2},x_5+\frac{1}{2}\}$. Along with the above superspace operations, the remaining generator of this five-dimensional (5-d) superspace group can be taken to be $\{+x_2+\frac{1}{2},x_1-\frac{1}{2},x_3,+x_5+\phi_1-\phi_2+\frac{1}{2},+x_4-\phi_1+\phi_2-\frac{1}{2}\}$. With the help of these superspace symmetry generating operations, it is now possible to derive the symmetry-constrained form of the 2-d displacive AMF describing the deviation of the As ions of the modulated structure from their underlying positions in the (001) planes of the ZrSiS-type average structure.

Systematic application of the above superspace generating operations leads to the following expression for the displacive AMF of the As sites:

$$\begin{aligned}\mathbf{U}_{As1,2}(\bar{x}_4=\mathbf{q}_1\cdot[\mathbf{r}_{As1,2}+\mathbf{t}],\bar{x}_5=\mathbf{q}_2\cdot[\mathbf{r}_{As1,2}+\mathbf{t}]\\ =\pm\mathbf{b}\varepsilon_{As}\cos2\pi(\bar{x}_4-\phi_1)\pm\mathbf{a}\varepsilon_{As}\cos2\pi(\bar{x}_5-\phi_2)\\ +\cdots\text{higher order harmonic terms}\ldots\end{aligned}\qquad(2)$$

where the '+' sign refers to the As1 atoms and the '−' sign to the As2 atoms. Experimentally, only the first-order $\mathbf{G}\pm\mathbf{q}_1$ and $\mathbf{G}\pm\mathbf{q}_2$ satellite reflections are observed (see Fig. 3a). This, however, we believe is again due to phason disorder rather than a necessarily sinusoidal AMF. In fact, for the purposes of deriving a plausible As–As dimerization pattern (see Fig. 6b), we have again assumed an inherently square-wave shape for the displacive AMF (see Fig. 6a), i.e., for $-\frac{1}{4}<(\bar{x}_4-\phi_1)<\frac{1}{4}$ along the $(\bar{x}_4-\phi_1)$ direction of hyper-space we ascribe a value of +1 to $\cos2\pi(\bar{x}_4-\phi_1)$ in Eq. (2) above and for $+\frac{1}{4}<(\bar{x}_4-\phi_1)<\frac{3}{4}$ we ascribe a value of −1. Likewise, in the $(\bar{x}_5-\phi_2)$ direction of hyper-space we ascribe a value of +1 to $\cos2\pi(\bar{x}_5-\phi_2)$ in Eq. (2) above when $-\frac{1}{4}<(\bar{x}_5-\phi_2)<\frac{1}{4}$ and a value of −1 otherwise. The values of these variables are represented by the pair of + and − values in the different regions of hyper-space

(see Fig. 6a). With such an assumption every As atom will then move the same amount along one of four possible $\langle 110 \rangle$ directions (see Fig. 6b). We choose $\varepsilon_{As}\sqrt{2} \times a \sim 0.22$ Å so that the As–As separation distance in a dimer is close to the ideal As–As single covalent bond distance of 2.44 Å.

The shift of any particular As atom can then be derived from Fig. 6a by calculating the local values of $(\bar{x}_4 - \phi_1)$ and $(\bar{x}_5 - \phi_2)$. Fig. 6b, for example, shows the predicted resultant $7\mathbf{a} \times 7\mathbf{b}$ real space As distribution that results if we take ε as $\frac{2}{7} = 0.286$ exactly and $\phi_1 = \phi_2 = 0$ (equivalent to taking a particular section through hyperspace. The apparent residual supercell symmetry of Fig. 6b is of no particular significance. It is simply a consequence of the above choice for ϕ_1 and ϕ_2). Note that 50 out of 98 As atoms are then involved in an As–As dimer. Note also that reversing the sign of the As2 shifts (represented by the unfilled circles) relative to those of the As 1 shifts (represented by the filled circles) in Fig. 6b destroys most of these dimers, i.e., the observed characteristic extinction condition is indeed consistent with the preferential formation of As–As dimers. Finally, note that individual $\langle 110 \rangle$ strings in Fig. 6b bear close similarities to those shown in Fig. 5.

Clearly, the experimental observation of continuous diffuse rods along the $\mathbf{c}^*$ direction of reciprocal space means that there can be no correlation from one such (001) plane to the next. One way of describing this disorder would be to let the global phases vary randomly from one (001) As layer to the next, i.e., to randomly shift the origin of superspace from that shown in Fig. 6a to some other starting position. Corresponding $7\mathbf{a} \times 7\mathbf{b}$ real space As distributions can then be easily generated. All, however, show similar characteristics to Fig. 6b.

At this stage, it is important to re-emphasize that Fig. 6b provides a plausible model (but only a model) of the As–As shifts responsible for the observed diffuse scattering and raises additional questions as to local As–As bonding which cannot be answered definitively from the currently available experimental and theoretical data. It is acknowledged, for example, that not only are 2.44 Å As–As dimers apparent in Fig. 6b but also shortened ($\sim$2.67 Å) As–As separation distances between As atoms not associated with dimer formation.

The question of how the 1- and 2-d patterns of As–As dimerization represented by Figs. 5 and 6 can simultaneously coexist as required by the experimental observation of coexisting diffuse sheets and diffuse rods remains. Likewise, do the questions of how the Th and Se ions react to the local formation of As–As dimers and why the observed diffuse streaking in Fig. 2a has the detailed shape it does. To attempt to answer such questions, however, would almost certainly require large-scale Monte-Carlo-type simulations well beyond the scope of the current contribution. While questions thus still remain open, it seems clear that the structural origin of the low-temperature Kondo effect in ThAsSe can be ascribed to the gradual condensation of a CDW associated with As–As dimerization.

References

[1] J. Schoenes, W. Basca, F. Hulliger, Solid State Commun. 68 (1988) 287.
[2] J. Leciejewicz, A. Zygmunt, Phys. Status Solidi (a) 13 (1972) 657.
[3] A. Wojakowski, Z. Henkie, Z. Kletowski, Phys. Status Solidi (a) 14 (1972) 517.
[4] A. Wojakowski, Z. Henkie, Acta Phys. Pol. A 52 (1977) 40.
[5] J. Brunner, M. Erbudak, F. Hulliger, Solid State Commun. 38 (1981) 841.
[6] W. Reim, J. Schoenes, F. Hulliger, Physica B 130 (1985) 64.
[7] Z. Henkie, R. Fabrowski, A. Wojakowski, J. Alloys Compd. 219 (1995) 248.
[8] Z. Henkie, T. Cichorek, A. Pietraszko, R. Fabrowski, A. Wojakowski, B.S. Kuzhel, L. Kepinski, L. Krajczyk, A. Gukasov, P. Wisniewski, J. Phys. Chem. Solids 59 (1998) 385.
[9] Z. Henkie, T. Cichorek, R. Fabrowski, A. Wojakowski, B.S. Kuzhel, Cz. Marucha, M.S. Szczepaniak, J. Tadla, Physica B 281–282 (2000) 226.
[10] Z. Henkie, A. Pietraszko, A. Wojakowski, L. Kepinski, T. Cichorek, J. Alloys Compd. 317–318 (2001) 52.
[11] J. Kondo, Prog. Theor. Phys. Osaka 32 (1964) 37.
[12] J.A. Wilson, F.J. Di Salvo, S. Mahajan, Adv. Phys. 24 (1975) 117.
[13] M.B. Maple, R.P. Dickey, J. Herrmann, M.C. de Andrade, E.J. Freeman, D.A. Gajewski, R. Chau, J. Phys.: Condens. Matter 8 (1996) 9773.
[14] D.L. Cox, A. Zawadowski, Adv. Phys. 47 (1998) 599.
[15] F. Hulliger, in: F. Lévy (Ed.), Structural Chemistry of Layer-type Phases, Reidel, Dordrecht, 1976, p. 258.
[16] R.L. Withers, J.A. Wilson, J. Phys. C 19 (1986) 4809.
[17] R.L. Withers, J.G. Thompson, in: P.L. Gai (Ed.), In Situ Microscopy in Materials Research, Kluwer, Boston, 1997, pp. 301–330 (Chapter 13).
[18] F. Hulliger, J. Less-Common Metals 16 (1968) 113.
[19] A.-K. Larsson, R.L. Withers, L. Stenberg, J. Solid State Chem. 127 (1996) 222.
[20] T.R. Welberry, R.L. Withers, Phys. Chem. Miner. 17 (1990) 117.
[21] R.L. Withers, J.W. Steeds, J. Phys. C 20 (1987) 4019.
[22] F.J. Brink, R.L. Withers, L. Norén, J. Solid State Chem. 166 (2002) 73.
[23] B.D. Butler, T.R. Welberry, Acta Crystallogr. A 49 (1993) 736.
[24] F.J. Brink, R.L. Withers, J.G. Thompson, J. Solid State Chem. 155 (2000) 359.
[25] S. Bénazeth, D. Carré, P. Laruelle, Acta Crystallogr. B 38 (1982) 33.
[26] A. Grzechnik, J.Z. Zheng, D. Wright, W.T. Petuskey, P.F. McMillan, J. Phys. Chem. Solids 57 (1996) 1625.
[27] L. Norén, R.L. Withers, F. Javier García-García, A.-K. Larsson, Solid State Sci. 4 (2002) 27.
[28] R.L. Withers, S. Schmid, J.G. Thompson, Prog. Solid State Chem. 26 (1998) 1.
[29] C.J. Bradley, A.P. Cracknell, The Mathematical Theory of Symmetry in Solids, Clarendon, Oxford, 1972.
[30] J.M. Pérez-Mato, G. Madariaga, F.J. Zuniga, A. Garcia Arribas, Acta Crystallogr. A 43 (1987) 216.
[31] J.M. Pérez-Mato, in: J.M. Pérez-Mato, F.J. Zuniga, G. Madariaga (Eds.), Methods of Structural Analysis of Modulated Structures and Quasicrystals, World Scientific, Singapore, 1991, pp. 117–218.